CrossMark

ORIGINAL ARTICLE

Characterization of [11C]Lu AE92686 as a PET radioligand for phosphodiesterase 10A in the nonhuman primate brain

Kai-Chun Yang[1] · Vladimir Stepanov[1] · Nahid Amini[1] · Stefan Martinsson[1] ·
Akihiro Takano[1] · Jacob Nielsen[2] · Christoffer Bundgaard[3] · Benny Bang-Andersen[3] ·
Sarah Grimwood[4] · Christer Halldin[1] · Lars Farde[1,5] · Sjoerd J. Finnema[1,6]

Abstract

Purpose [11C]Lu AE92686 is a positron emission tomography (PET) radioligand that has recently been validated for examining phosphodiesterase 10A (PDE10A) in the human striatum. [11C]Lu AE92686 has high affinity for PDE10A ($IC_{50} = 0.39$ nM) and may also be suitable for examination of the substantia nigra, a region with low density of PDE10A. Here, we report characterization of regional [11C]Lu AE92686 binding to PDE10A in the nonhuman primate (NHP) brain.

Methods A total of 11 PET measurements, seven baseline and four following pretreatment with unlabeled Lu AE92686 or the structurally unrelated PDE10A inhibitor MP-10, were performed in five NHPs using a high resolution research tomograph (HRRT). [11C]Lu AE92686 binding was

quantified using a radiometabolite-corrected arterial input function and compartmental and graphical modeling approaches.

Results Regional time-activity curves were best described with the two-tissue compartment model (2TCM). However, the distribution volume (V_T) values for all regions were obtained by the Logan plot analysis, as reliable cerebellar V_T values could not be derived by the 2TCM. For cerebellum, a proposed reference region, V_T values increased by ~30 % with increasing PET measurement duration from 63 to 123 min, while V_T values in target regions remained stable. Both pretreatment drugs significantly decreased [11C]Lu AE92686 binding in target regions, while no significant effect on cerebellum was observed. Binding potential (BP_{ND}) values, derived with the simplified reference tissue model (SRTM), were 13–17 in putamen and 3–5 in substantia nigra and correlated well to values from the Logan plot analysis.

Conclusions The method proposed for quantification of [11C]Lu AE92686 binding in applied studies in NHP is based on 63 min PET data and SRTM with cerebellum as a reference region. The study supports that [11C]Lu AE92686 can be used for PET examinations of PDE10A binding also in substantia nigra.

✉ Kai-Chun Yang
kai-chun.yang@ki.se

1 Department of Clinical Neuroscience, Center for Psychiatric Research, Karolinska Institutet, Karolinska University Hospital, Stockholm, Sweden

2 Synaptic Transmission, H. Lundbeck A/S, Valby, Denmark

3 Discovery Chemistry and DMPK, H. Lundbeck A/S, Valby, Denmark

4 Neuroscience and Pain Research Unit, Pfizer Inc., Cambridge, MA, USA

5 Personalized Health Care and Biomarkers, AstraZeneca PET Science Center at Karolinska Institutet, Stockholm, Sweden

6 Present address: Department of Radiology and Biomedical Imaging, Yale University, New Haven, CT, USA

Introduction

Phosphodiesterase 10A (PDE10A) is a member of the cyclic nucleotide phosphodiesterase family and modulates intracellular signal transduction by catabolizing cyclic adenosine monophosphate (cAMP) and guanosine monophosphate (cGMP) [1]. The intracellular enzyme PDE10A is almost

exclusively expressed in GABAergic medium spiny neurons of the striatum, where it is distributed to both cell bodies and processes at presynaptic sites within globus pallidus (GP) and substantia nigra (SN) [1–5]. The localization in the basal ganglia and interaction with dopaminergic neurotransmission [5, 6] suggest that PDE10A may play a role in striatal functions such as cognitive and motor abilities [1, 6, 7]. PDE10A has, therefore, been considered as a potential therapeutic target for several neuropsychiatric disorders, including schizophrenia, bipolar disorder, Huntington's disease and Parkinson's disease [1, 7, 8].

Numerous potential radioligands for imaging of PDE10A binding by positron emission tomography (PET) have been suggested and several have been examined in nonhuman primates (NHP) or in humans [8–19]. Most of these radioligands provide adequate target-to-background signal for the striatum and GP, but so far, radioligand binding in the SN has been examined only for [18F]JNJ-42259152 or [11C]IMA107. Both studies report binding potential (BP_{ND}) values of approximately 0.5 for SN in healthy human subjects with corresponding striatal BP_{ND} values of 3.5 or 2.2, respectively [8, 16]. This low BP_{ND} value might limit the application of these radioligands for quantitative examinations of PDE10A binding in SN [20]. Considering that the SN is a key nucleus in relation to the basal ganglia [21], and that regional differences in PDE10A functioning may be a part of the pathophysiology of neuropsychiatric disorders [2, 5, 6], it is important to develop a PET methodology enabling quantification of PDE10A binding in the SN of the primate brain.

[11C]Lu AE92686 is a recently developed radioligand with high affinity for PDE10A ($IC_{50} = 0.39$ nM). An evaluation of the radioligand in humans has previously been reported [9]. The characteristics of this radioligand are promising, with striatal BP_{ND} value around 7.5 in humans [9], which is higher than those reported for other PDE10A radioligands (typical range: 2–5) [8–19]. Preliminary examination of [11C]Lu AE92686 in cynomolgus monkeys has suggested that [11C]Lu AE92686 binding is high in the striatum (BP_{ND} around 6.5), and the specificity of binding was demonstrated by dose-dependent reduction in uptake of [11C]Lu AE92686 following the administration of PDE10A inhibitor MP-10 [9]. However, the initial study in monkeys did not include a full kinetic evaluation of [11C]Lu AE92686 or examination of binding in the SN.

The aim of the present study was to further characterize the binding properties of [11C]Lu AE92686 in NHPs. To enable examinations of PDE10A binding in the SN, PET measurements were conducted using the High Resolution Research Tomograph (HRRT). For full kinetic quantification of [11C]Lu AE92686 binding, a metabolite-corrected arterial input function (AIF) was obtained. Moreover, pretreatment experiments with unlabeled Lu AE92686 or the structurally unrelated PDE10A inhibitor MP-10 were performed to further characterize the specificity of binding and to evaluate the suitability of cerebellum as a reference region.

Materials and methods

Subjects

The study was approved by the Animal Research Ethical Committee of the Northern Stockholm region (Dnr N452/11, N632/12, N633/12 and N185/14). Five female cynomolgus monkeys (*Macaca fascicularis*) with body weight: 6.4 ± 1.7 kg (mean±standard deviation (SD)), for all following values with the same format) were included. The caring and experimental procedures were performed according to the 'Guidelines for planning, conducting and documenting experimental research' (Dnr 4820/06-600) of Karolinska Institutet and the 'Guide for the Care and Use of Laboratory Animals: Eighth Edition' [22].

Preparation of [11C]Lu AE92686

[11C]Lu AE92686 was prepared according to procedures reported previously [9] as described in Online Resource 1.

Study design

A total of 11 PET measurements with arterial blood sampling were performed on seven experimental days. Each monkey underwent one baseline PET measurement on each experimental day and on four experimental days a consecutive PET measurement was conducted after pretreatment with MP-10 (1.5 mg/kg, NHP1 and NHP2) or Lu AE92686 (0.5 mg/kg or 2.0 mg/kg, NHP1). The interval between the two PET measurements on the same day was approximately 3 h.

Test drug administration

MP-10 [23] was formulated in a mixture of PEG 400 (25 %, v/v) and 0.9 % saline (75 %, v/v), and Lu AE92686 was formulated in a mixture of 10 % hydroxypropyl beta cyclodextrin dissolved in phosphate buffered saline (PBS). All drug solutions were infused (~1 mL/kg) over 15 min, starting 45 min before injection of [11C]Lu AE92686.

PET experimental procedures

Anesthesia was initiated by intramuscular injection of ketamine hydrochloride (~10 mg/kg) and maintained by sevoflurane (2–8 %). PET measurements were conducted in the HRRT; a six-minute transmission scan (using a single Cesium-137 source) was followed by the acquisition of list-mode data for 123 min after a bolus injection of [11C]Lu AE92686.

Arterial blood samples were collected continuously during the first 3 min after radioligand injection by using an

automated blood sampling system, and subsequent arterial blood samples were taken manually. Manual samples included one sample for determination of protein binding (5 min before radioligand injection), 14 samples (at 0.5, 1.0, 1.5, 2.0, 2.5, 3.0, 4.0, 5.0, 8.0, 15, 30, 60, 90 and 120 min) for measurement of blood and plasma radioactivity and seven samples (at 2.5, 4.0, 15, 30, 60, 90 and 120 min) for radiometabolite analyses. In the pretreatment experiments, five additional blood samples (at 15, 30, 60, 90 and 120 min) were taken for determination of plasma drug concentrations.

Blood samples analysis

The free fraction (f_p) of [^{11}C]Lu AE92686 in plasma was estimated by ultrafiltration, and the percentages of radioactivity for unchanged radioligand and radiometabolites in plasma were determined by reversed-phase high-performance liquid chromatography (HPLC) according to procedures reported previously [14, 24]. Plasma drug concentrations were determined using ultra performance liquid chromatography (UPLC) followed by tandem mass spectrometry (MS/MS) detection according to procedures reported previously [25]. The details of the blood sample analysis are described in Online Resource 1.

Image data analysis

Each monkey underwent magnetic resonance imaging (MRI), and the images were used for anatomical guidance to define regional volumes of interest (VOIs). PET images were preprocessed according to previously reported methods [26] with reconstructed image frames binned as: 9×20 s, 3×60 s, 5×180 s and 17×360 s. Each subject's baseline blood flow by dominated PET image (average of time frames corresponding to 0–9 min) was coregistered manually to their individual MRI image, and the resulting transformation matrices were applied to the corresponding dynamic PET image. For pretreatment studies, the transformation parameters of the baseline measurements were applied to both of the two PET measurements performed on the same day.

Six VOIs were defined, including three striatal regions: putamen, caudate nucleus (CN) and ventral striatum (VS), two extrastriatal regions: GP and SN and one reference region: cerebellum. A decay-corrected time–activity curve (TAC) was generated for each VOI from the coregistrated dynamic PET data and radioactivity was expressed as standardized uptake values (SUV), which were calculated from the radioactivity concentration as [kBq/cm^3] / (radioactivity injected [MBq] / body weight [kg]). Specific binding was defined as radioactivity in target region minus radioactivity in cerebellum.

Quantification of PET signals

Kinetic analysis was performed by applying the 1-tissue compartment model (1TCM) and the 2-tissue compartment model (2TCM). Logan plot analysis [27] was also applied and the starting time of linearization (t^*) was decided for each VOI in each experiment separately by examining total distribution volume (V_T) and identifiability of V_T based on different t^* ranging from 6 min to a time point with five time frames remaining until the end of PET measurement. In addition to the acquisition of 123 min data, the effects of the PET measurement duration on V_T estimates were examined by varying the time interval from 0 to 33 min to 0–117 min with one time frame increments. BP_{ND} was derived by three approaches, the indirect method using the following equation

$$BP_{ND} = \frac{\text{Regional } V_T - \text{Cerebellar } V_T}{\text{Cerebellar } V_T}, \qquad (1)$$

and two reference tissue models: the simplified reference tissue model (SRTM) [28] and Logan reference tissue model (Loganref) [29]. The efflux rate constant k_2' in Loganref was derived by using SRTM and couple fitting of all target regions except SN (excluded due to its relatively high noise levels). The t^* for Loganref was 27 min, based on the results of the Logan plot analysis.

All analyses of imaging data were performed using PMOD (version 3.403; PMOD Technologies, Zurich, Switzerland). The fits obtained by different models were evaluated by the model selection criterion (MSC) [30], for which a higher value indicates a better fit. The identifiability of parameters was expressed by the percentage of the coefficient of variation (%COV) calculated according to the following equation

$$\%COV = (\text{Standard error of estimates}/\text{Estimates of parameters}) \times 100. \quad (2)$$

Poor identifiability was defined as %COV > 10 %. For the pretreatment studies, Lassen plots [31] were applied to estimate the nondisplaceable distribution volume (V_{ND}) and PDE10A occupancy. Due to the significant difference of the plasma free fraction (f_p) before and after pretreatment (see results section), the evaluation of pretreatment effect was based on V_T or V_{ND} values normalized for f_p as V_T/f_p or V_{ND}/f_p, respectively.

Results

All PET measurements were performed according to the study protocol and no significant adverse effects were observed during the pretreatment experiments.

Radiochemistry

The radiochemical purity of $[^{11}C]$Lu AE92686 was higher than 99 %, and the average specific radioactivity at time of injection was 1062 GBq/μmol (range: 609–1457 GBq/μmol), corresponding to a mean injected mass of 0.07 μg (range: 0.04–0.12 μg).

Plasma radioactivity and radiometabolite analysis

$[^{11}C]$Lu AE92686 was rapidly metabolized and parent compound fraction was 18 ± 4 % of the plasma radioactivity at 60 min after injection (Fig. 1a). At 15 min after injection, three main radiometabolite fractions ($[^{11}C]$M1 – $[^{11}C]$M3) eluted earlier than $[^{11}C]$Lu AE92686 (Fig 1b). At later time points, $[^{11}C]$M1 and $[^{11}C]$M2 could not be separated and the combined fraction increased with time until 90 min post injection (Fig. 1a). In addition, several small radiometabolite fractions ($[^{11}C]$M4) eluted later than $[^{11}C]$Lu AE92686 (Fig. 1c). The time course

of plasma radioactivity of parent $[^{11}C]$Lu AE92686 at baseline measurements ($n = 7$) is presented in Fig. 1d.

Quantification of $[^{11}C]$Lu AE92686 receptor binding

After intravenous injection of $[^{11}C]$Lu AE92686 at baseline conditions, there was a rapid increase of radioactivity in regions known to express PDE10A (Fig. 2, left column). The TACs for target regions and cerebellum are shown in Fig. 3a. Specific binding, when defined as the difference between radioactivity in target region and the cerebellum, reached maximum values within 60 min after injection for all target regions (Fig. 3b).

The regional TACs were first interpreted by the 1TCM and 2TCM. For target regions, both models appeared to describe experimental data equally well. For cerebellum, the 2TCM described TACs better than the 1TCM (Fig. 4a). A summary of model parameters is given in Table 1. There were statistically higher MSC values for the 2TCM than for 1TCM in SN ($P < 0.01$) and in cerebellum ($P < 0.0001$) as well as when
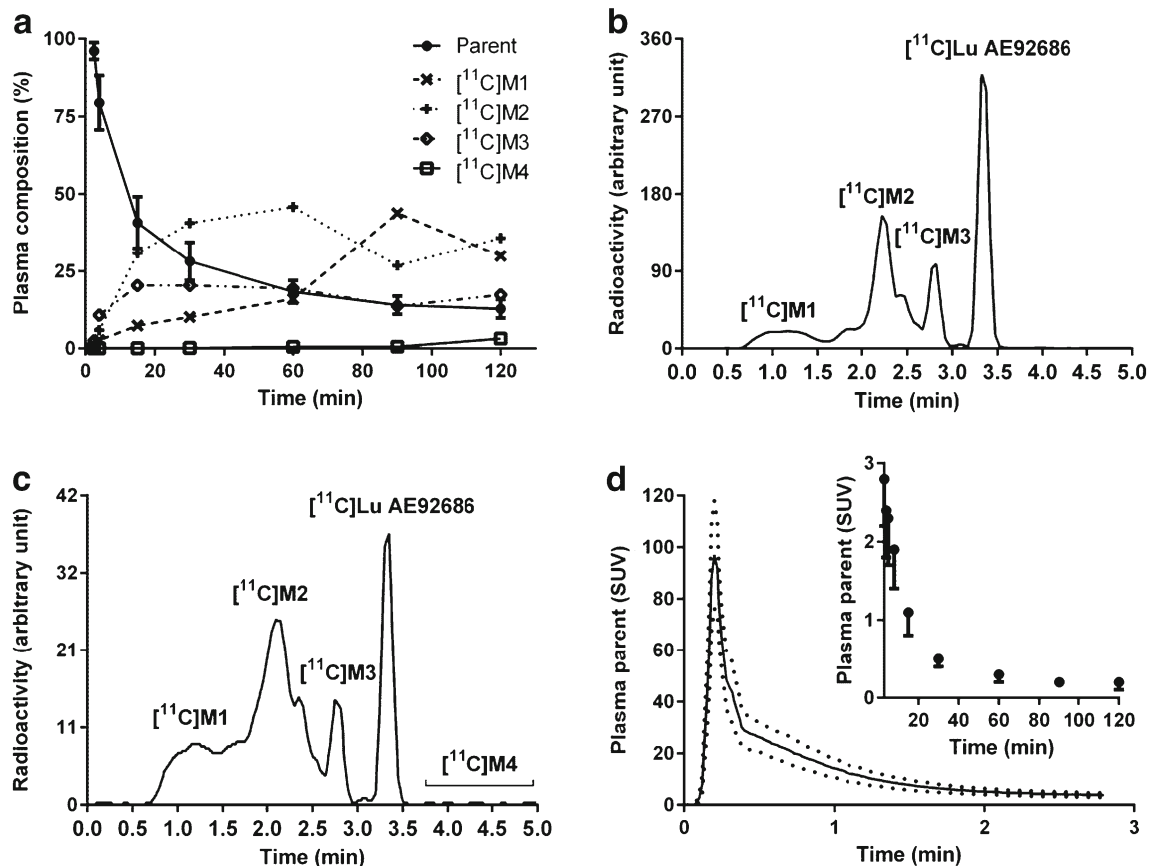
Fig. 1 Composition of radioactivity in arterial plasma samples after $[^{11}C]$Lu AE92686 injection in baseline experiments. (**a**) Plasma composition of unchanged radioligand (mean±SD) and radiometabolites (mean) fractions over time ($n = 7$) (**b**) Representative HPLC radiochromatogram of plasma content 15 min post injection (**c**) HPLC: 60 min post injection (**d**) Radiometabolite-corrected arterial input function of $[^{11}C]$Lu AE92686 ($n = 7$) from 0 to 3 min (mean±SD); inset shows values from 3 to 120 min (mean – SD), expressed in standardized uptake value (SUV)

Fig. 2 Magnetic resonance images and corresponding coregistrated PET summation images (average of frames from 9 to 123 min) of [^{11}C]Lu AE92686 during baseline (mean of three baseline experiments) and three pretreatment conditions in NHP1. (**a**) Axial (top) and coronal (bottom) view of images at the level of striatum (**b**) Axial (top) and coronal (bottom) view of images at the level of substantia nigra; note the difference in the range of the standardized uptake value (SUV) colour bars between (**a**) and (**b**)
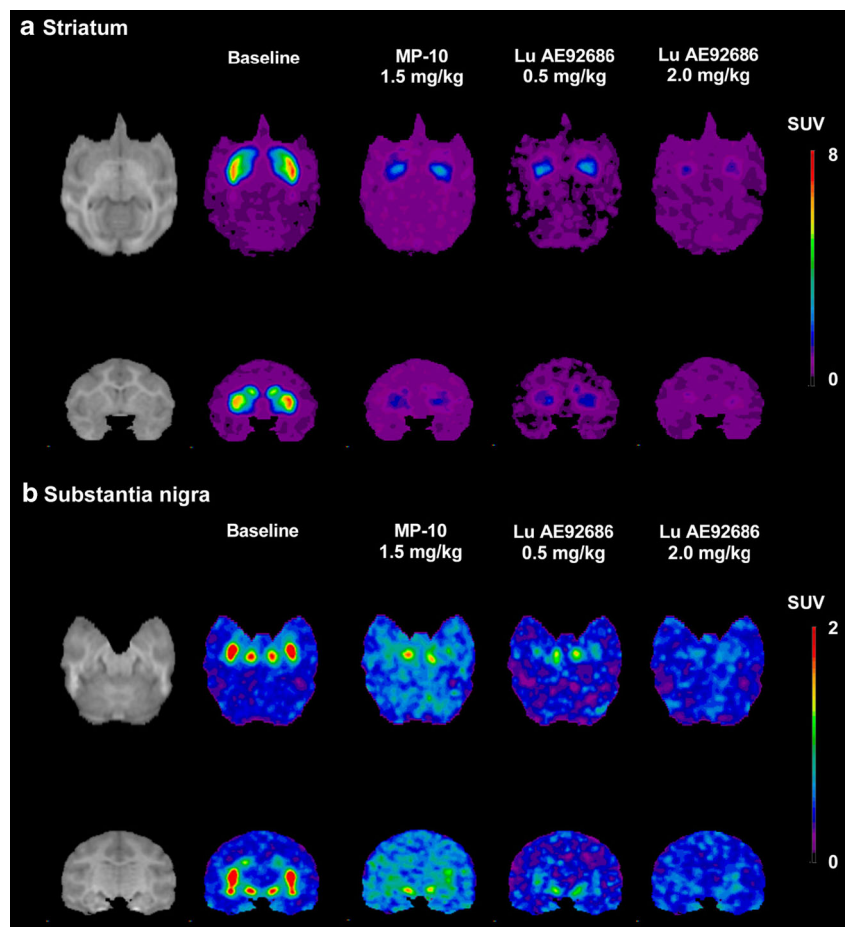
pooling all six regions (2.8 ± 1.3 and 3.1 ± 1.3, $P < 0.0001$). For the 2TCM, mean K_1 values ranged from 0.06 to 0.11 with mean %COV from 3 to 17 %. The estimated k_3, k_4, K_1/k_2 and k_3/k_4 values suffered from poor identifiability (%COV > 50 % in most fits). Furthermore, the 2TCM had poor V_T identifiability (%COV > 10 %) in all fits for the cerebellum and in a few fits for the target regions (four of 35 fits).

Data were also interpreted by Logan plot analysis with AIF (Fig. 4b), and identifiable V_T estimates (%COV $\leq$ 10 %) could be derived for all regions and all subjects. V_T values by Logan plot analysis correlated with those obtained by the 2TCM with %COV $\leq$ 10 % (Pearson $r > 0.99$, $P < 0.0001$, $n = 30$). However, the values were slightly lower than those obtained using 2TCM (-6.3 ± 2.6 %). When comparing the two
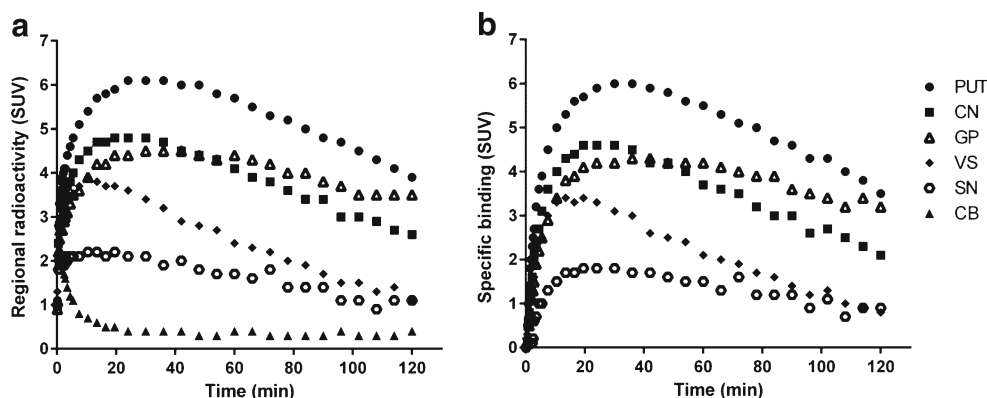
Fig. 3 Time-activity course of radioactivity in brain for baseline experiments ($n = 7$), expressed in standardized uptake value (SUV). (**a**) Mean regional brain radioactivity concentrations in five target regions: putamen (PUT), caudate nucleus (CN), globus pallidum (GP), ventral striatum (VS), and substantia nigra (SN) as well as one reference region: cerebellum (CB) (**b**) Mean regional specific binding (radioactivity in target region - radioactivity in cerebellum) in five target regions

Fig. 4 Representative kinetic modelling evaluation of $[^{11}C]$Lu AE92686 in one NHP. (**a**) One-tissue compartment model (1TCM) fits and two-tissue compartment model (2TCM) fits in the caudate nucleus (as in putamen and globus pallidus), substantia nigra (as in ventral striatum), and cerebellum (**b**) Corresponding Logan plot analysis described the data adequately for all regions
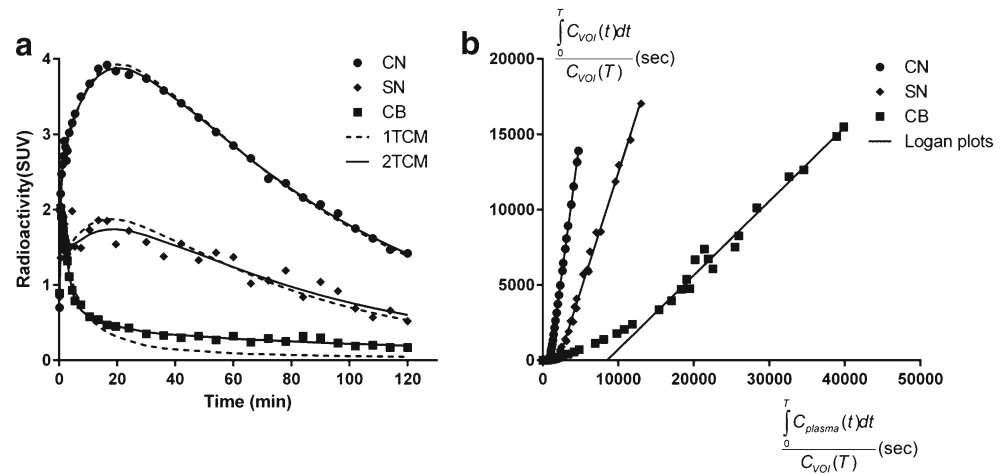
models, the equation for the linear regression analysis was y = 0.934x + 0.015 ($R^2 > 0.99$). In the following, the analyses were based on the V_T values obtained by Logan plot analysis, since this model provided well identifiable values for all regions, including cerebellum.

In target regions and PET data set of less than 63 min, V_T estimates were unstable (high variation with different t^*) and poorly identifiable V_T estimates were obtained for several regions (13 of 35 fits for 33 min data). The V_T values for the cerebellum increased prominently with longer PET measurement duration as V_T values for 33 min, 93 min and 123 min data accounted for 78.9 ± 3.4 %, 131.8 ± 16.6 % and 131.8 ± 10.4 % of the V_T obtained for 63 min data, respectively (Fig. 5a and b). The V_T values of target regions remained stable after increasing PET measurement duration, and V_T values for 123 min data accounted for 101.3 ± 9.3 % of the V_T obtained for 63 min data (Fig. 5b). To minimize the possible influence of radiometabolites (see discussion section), 63 min was chosen as the preferred PET measurement duration.

Table 1 Parameters estimated by the 1-tissue compartment model (1TCM) and the 2-tissue compartment model (2TCM) in baseline PET measurements ($n = 7$)

	1TCM		2TCM				
	V_T (ml · cm^{-3}) %COV	MSC	V_T (ml · cm^{-3}) %COV	MSC	K_1[a] %COV	k_3 (min^{-1}) %COV	k_4 (min^{-1}) %COV
PUT	11.9 ± 3.8	4.2 ± 0.7	11.8 ± 3.7	4.3 ± 0.5	0.11 ± 0.02	0.55 ± 0.36	0.158 ± 0.105
	2 ± 1		2 ± 1		6 ± 5	61 ± 43	79 ± 67[b]
CN	7.5 ± 2.4	3.8 ± 0.9	7.4 ± 2.4	4.0 ± 0.6	0.10 ± 0.02	0.34 ± 0.21[d]	0.137 ± 0.094[d]
	2 ± 1		4 ± 6		4 ± 2	69 ± 52[d]	48 ± 47[d]
GP	10.3 ± 3.1	2.9 ± 0.7	10.3 ± 3.1	3.0 ± 0.5	0.08 ± 0.02	0.49 ± 0.48	0.058 ± 0.024[b]
	4 ± 1		5 ± 2		17 ± 13	124 ± 8	113 ± 34[b]
VS	3.8 ± 1.2	2.2 ± 0.4	4.0 ± 1.3[b]	2.3 ± 0.2	0.10 ± 0.03	0.44 ± 0.63	0.080 ± 0.036[b]
	3 ± 1		4 ± 2[b]		9 ± 6	124 ± 128	63 ± 35[b]
SN	2.7 ± 0.9	0.8 ± 0.6	2.6 ± 0.7[b]	1.1 ± 0.5*	0.06 ± 0.01[b]	0.26 ± 0.33	0.038 ± 0.009[b]
	7 ± 3		7 ± 2[b]		11 ± 4[b]	82 ± 29	38 ± 23[b]
CB	0.2 ± 0.1	2.8 ± 0.5	0.9 ± 0.4[e]	4.2 ± 0.6*	0.09 ± 0.02	0.02 ± 0.01	0.003 ± 0.004[c]
	6 ± 2		28 ± 16[e]		3 ± 1	23 ± 6	144 ± 130[c]

Data presented as mean±SD

V_T total distribution volume, *COV* the coefficient of variation, *MSC* model selection criterion, *PUT* Putamen, *CN* Caudate nucleus, *GP* Globus pallidum, *VS* Ventral striatum, *SN* Substantia nigra, *CB* Cerebellum

[a] unit = ml · min^{-1} · cm^{-3}

[b] $n = 6$; [c] $n = 5$; [d] $n = 4$; [e] $n = 3$ (excluding data with %COV > 50 % for V_T or K_1 and data with %COV > 500 % for k_3 or k_4)

*$P < 0.05$ (two tailed, comparing the results for 1TCM and 2TCM by paired t-test)

Pretreatment experiments

Five blood samples were obtained within the period of the PET measurements for assessment of the plasma concentration of the pretreatment drugs. The mean plasma concentrations were 685 and 749 ng/mL after injection of MP-10, 109 ng/mL after injection of Lu AE92686 0.5 mg/kg and 388 ng/mL after Lu AE92686 2.0 mg/kg. (Fig. S1 in Online Resource 2). The metabolic rate of [11C]Lu AE92686 after pretreatment was similar to baseline conditions (Fig. S2 in Online Resource 2).

Following administration of MP-10 or Lu AE92686, radioactivity was lower in all target regions when compared to baseline (Fig. 6a–c). Radioactivity concentrations in the cerebellum were similar between baseline and pretreatment conditions (Fig. 6d). The pooled K_1 values obtained by the 2TCM were 0.092 ± 0.029 at baseline conditions and 0.221 ± 0.114 ($P < 0.0001$) after pretreatment, suggesting a drug effect on blood flow.

The plasma free fraction (f_p) of [11C]Lu AE92686 was 0.06 ± 0.01 during baseline conditions, whereas it was higher after administration of MP-10 (0.14 and 0.09) or Lu AE92686 (0.07 and 0.15 for 0.5 mg/kg and 2.0 mg/kg, respectively). Both MP-10 and Lu AE92686 induced a significant reduction in V_T/f_p in target regions, and the reduction in V_T/f_p was larger after the higher dose of Lu AE92686 (Table 2). For the cerebellum, there was no statistical significant difference (4.8 ± 15.4 %, $P = 0.55$) in V_T/f_p between baseline (8.6 ± 2.5) and pretreatment (9.0 ± 2.5) conditions (Table 2).

The PDE10A occupancy after pretreatment was estimated using Lassen plots (Fig. 7). In all studies the goodness of fit (R^2) for linear fitting was higher than 0.90. In the two NHPs receiving MP-10, the estimated PDE10A occupancy was 93 % and 95 % (Fig. 7a and b). The estimated PDE10A occupancy by Lu AE92686 was 84 % and 96 % after 0.5 mg/kg and 2.0 mg/kg, respectively (Fig. 7c and d). For these four pretreatment experiments, there was a trend towards V_{ND}/f_p values (8.6 ± 2.5) being lower than V_T/f_p values for the cerebellum at baseline conditions (15.2 ± 5.7) ($P = 0.08$).

Reference tissue models

The cerebellum was used as a reference region, since there was no significant reduction of binding after pretreatment. The baseline V_T values of target regions and cerebellum are given in Table 3. BP_{ND} values could be derived in all experiments by using SRTM or Loganref (Fig. 8a and b). The baseline BP_{ND} values calculated by the different models are presented in Table 3. Since the results of the two reference tissue models were comparable (absolute difference: 5.0 ± 4.4 %, Pearson $r > 0.99$ and $P < 0.0001$), only the results of the SRTM are reported in the following sections.

The BP_{ND} values calculated by SRTM in the baseline measurements were lower than those derived indirectly by Logan plot analysis (-19.7 ± 18.2 %, median: -23.3 %) and the difference became mildly positive in pretreatment experiments (5.8 ± 16.8 %, median: 1.5 %) (Fig. 8c). The negative difference (%) became larger at higher BP_{ND} values both for baseline measurements (Pearson $r = -0.88$ and $P < 0.0001$) and pretreatment measurements (Pearson $r = -0.50$ and $P = 0.03$). There was a significant correlation between BP_{ND} values calculated by Logan plot analysis and SRTM in the baseline measurements (Pearson $r = 0.95$, $P < 0.0001$) and in the pretreatment measurements (Pearson $r = 0.98$, $P < 0.0001$). When pooling baseline and pretreatment data, the equation for the linear regression analysis was y = $0.601x + 1.295$ ($R^2 = 0.95$) (Fig. 8d).

Discussion

In the current study, we conducted kinetic analyses of [11C]Lu AE92686 to evaluate the suitability of this radioligand for PET examinations of regional PDE10A binding in the monkey brain. There are three main observations: first, regional [11C]Lu AE92686 binding could be quantified in the striatum, GP and SN using Logan plot analysis as well as reference tissue models. Second, pretreatment studies confirmed the specificity of [11C]Lu AE92686 binding to PDE10A, and there was no evident effect of pretreatment on PDE10A binding in the cerebellum. Third, an influence of blood–brain barrier (BBB) penetrating radiometabolites on brain radioactivity could not be excluded and was minimized by using PET data only for the first 63 min after injection. In conclusion, [11C]Lu AE92686 has potential for examinations of PDE10A binding not only in the striatum and GP but also in the SN in future NHP PET studies.

Kinetic analyses of [11C]Lu AE92686 suggested that both the 1TCM and 2TCM could describe the TACs for regions with high PDE10A binding. However, the TACs were best described with the 2TCM in regions with low or no specific binding such as SN or cerebellum. The results for the striatum and cerebellum are compatible with a previous evaluation of [11C]Lu AE92686 in humans, though the TACs for the human cerebellum were best described by the irreversible 2TCM in the previous study [9], we found no significant difference in MSC values between reversible and irreversible 2TCM. A possible explanation is that some small compartments may represent a larger part of the total signal in regions with low or no specific binding and, thus, are identified by the model.

Overall, the radioactivity in the cerebellum was about 10 % of radioactivity in the putamen (Fig. 3a). The low signal for the cerebellum could be a reason for poor identifiability of V_T values in this region when using 2TCM [9]. In contrast, Logan plot analysis provided less variable V_T values in all regions
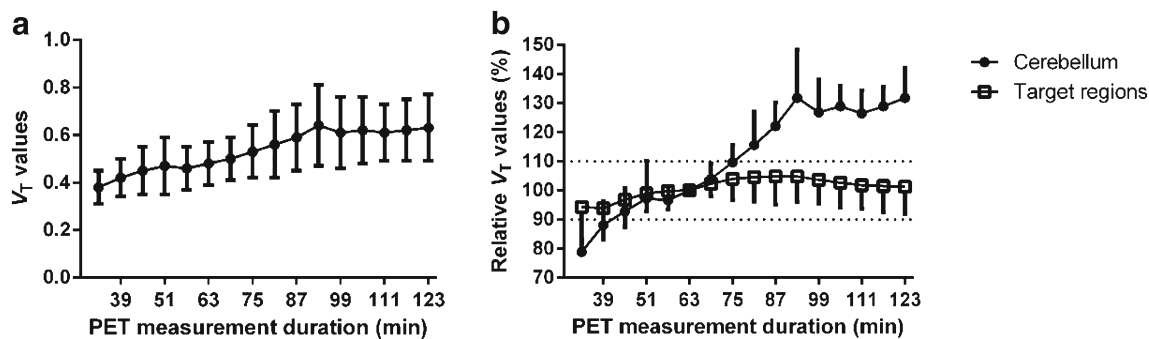
Fig. 5 Effect of PET measurement duration on V_T values derived by the Logan plot analysis; Relative V_T values (%) = [(V_T values by corresponding duration of PET measurement - V_T values by reference duration of PET measurement) / V_T values by reference duration of PET measurement] × 100 (**a**) Cerebellar V_T values (mean±SD) (**b**) Relative V_T values to 63 min data for target regions (mean − SD) and cerebellum (mean+SD)

with a %COV < 10 %. Therefore, the Logan plot analysis is the recommended quantification method for estimating V_T values by [^{11}C]Lu AE92686 in NHPs and in humans [9].

In agreement with a previous report in humans [9], there were no major differences between the two examined reference tissue models, SRTM and Loganref, used to quantify regional [^{11}C]Lu AE92686 binding. When considering the reference tissue model performance criteria recently proposed by Zanderigo and coworkers [32], it can be noted that the correlation between pooled BP_{ND} values of reference tissue models and Logan plot analysis was high (>0.95, proposed: >0.5) and the median percent difference of BP_{ND} values between reference tissue models and Logan plot analysis was

low (1.5 % to 23.3 %, proposed: <50 %). Fulfillment of these two criteria suggests that SRTM and Loganref may be used to quantify [^{11}C]Lu AE92686 binding with acceptable accuracy.

In addition to the two criteria mentioned above, the third proposed performance criterion is a slope of the linear regression line of BP_{ND} values between reference tissue models and AIF-based quantification method within the range of 0.7–1.3 (corresponding to a maximum relative difference ≤ 30 %) [32]. In the current study, the slope was 0.6 suggesting that the maximum relative difference in reference tissue models was higher than the proposed level. The deviation between the regression line and the line of identity is mainly driven by regions with high PDE10A density (Fig. 8c and d). Since

Fig. 6 Time-activity course for radioactivity in brain for baseline experiments (mean of three measurements) and corresponding pretreatment measurements of [^{11}C]Lu AE92686 in one NHP, expressed in standardized uptake value (SUV). Regional brain radioactivity concentrations in (**a**) caudate nucleus, (**b**) globus pallidus, (**c**) substantia nigra and (**d**) cerebellum
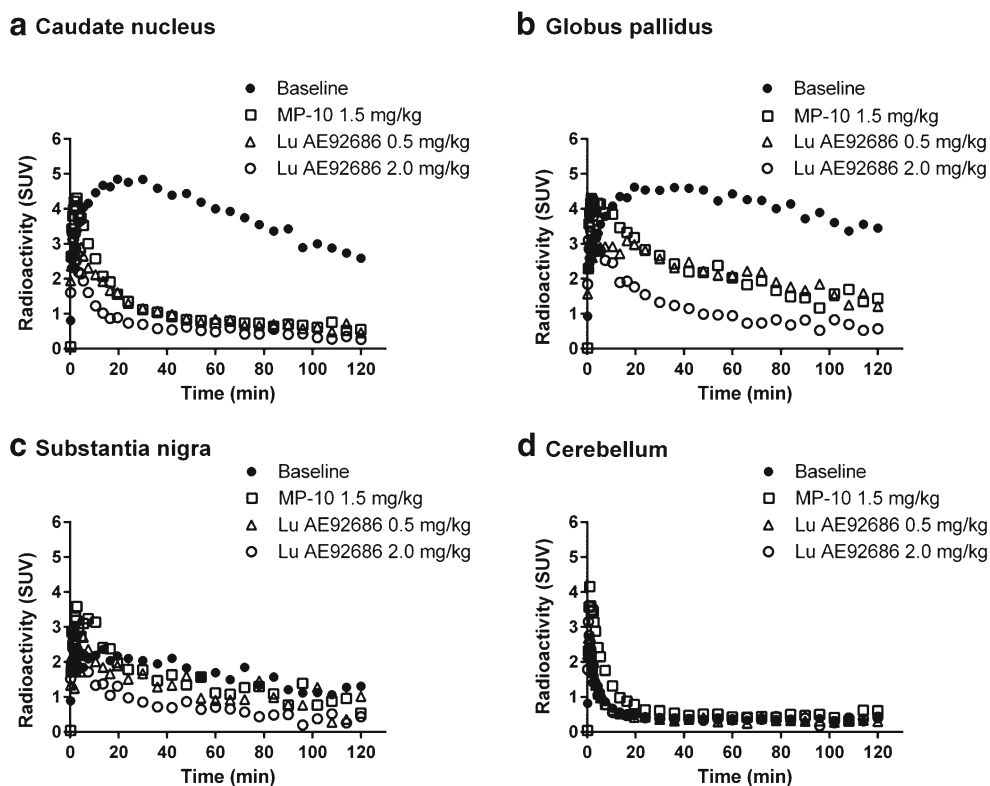
Table 2 Changes in regional V_T / f_p (%)[a] following three different pretreatment regimens

	MP-10 1.5 mg/kg	MP-10 1.5 mg/kg	Lu AE92686 0.5 mg/kg	Lu AE92686 2.0 mg/kg
PUT	−89.2	−87.9	−80.5	−93.7
CN	−88.0	−86.3	−76.4	−92.8
GP	−76.4	−76.2	−54.9	−90.3
VS	−81.6	−77.2	−66.2	−89.8
SN	−46.7	−43.2	−23.4	−75.8
CB	1.0	−3.5	26.3	−9.7

PUT Putamen, *CN* Caudate nucleus, *GP* Globus pallidum, *VS* Ventral striatum, *SN* Substantia nigra, *CB* Cerebellum

[a] Change in V_T / f_p (%) $= \left(\frac{\text{Pretreatment} - \text{Baseline}}{\text{Baseline}}\right) \times 100$

the current BP_{ND} values in target regions are relatively high (>15), a relatively large maximum difference in BP_{ND} estimates by SRTM can be anticipated. Similar observations have

previously been reported for several other radioligands, including [^{11}C]Cimbi-36, [^{11}C]WAY-100635 and [^{11}C]FLB 457 [24, 33–35]. As for these established radioligands, reference tissue models may be considered for quantification of [^{11}C]Lu AE92686 binding in NHP studies in particular when multiple PET measurements are performed on the same subject such as in pharmacological challenge studies [32, 34, 36].

The pretreatment studies in the current study extend reported work, which has been performed in NHP without AIF [9]. The high reduction of [^{11}C]Lu AE92686 binding in target regions after pretreatment with MP-10, a PDE10A inhibitor from a different structural class than Lu AE92686, supports the view that [^{11}C]Lu AE92686 binds specifically to PDE10A. In all pretreatment studies, the fit of the Lassen plots was good (R^2 from 0.93 to >0.99). These results suggest that the regional PDE10A occupancy was homogenous and that all five target regions have a similar V_{ND} [31].

In addition, pretreatment by MP-10 or Lu AE92686 did not significantly reduce the cerebellar V_T/f_p values. The
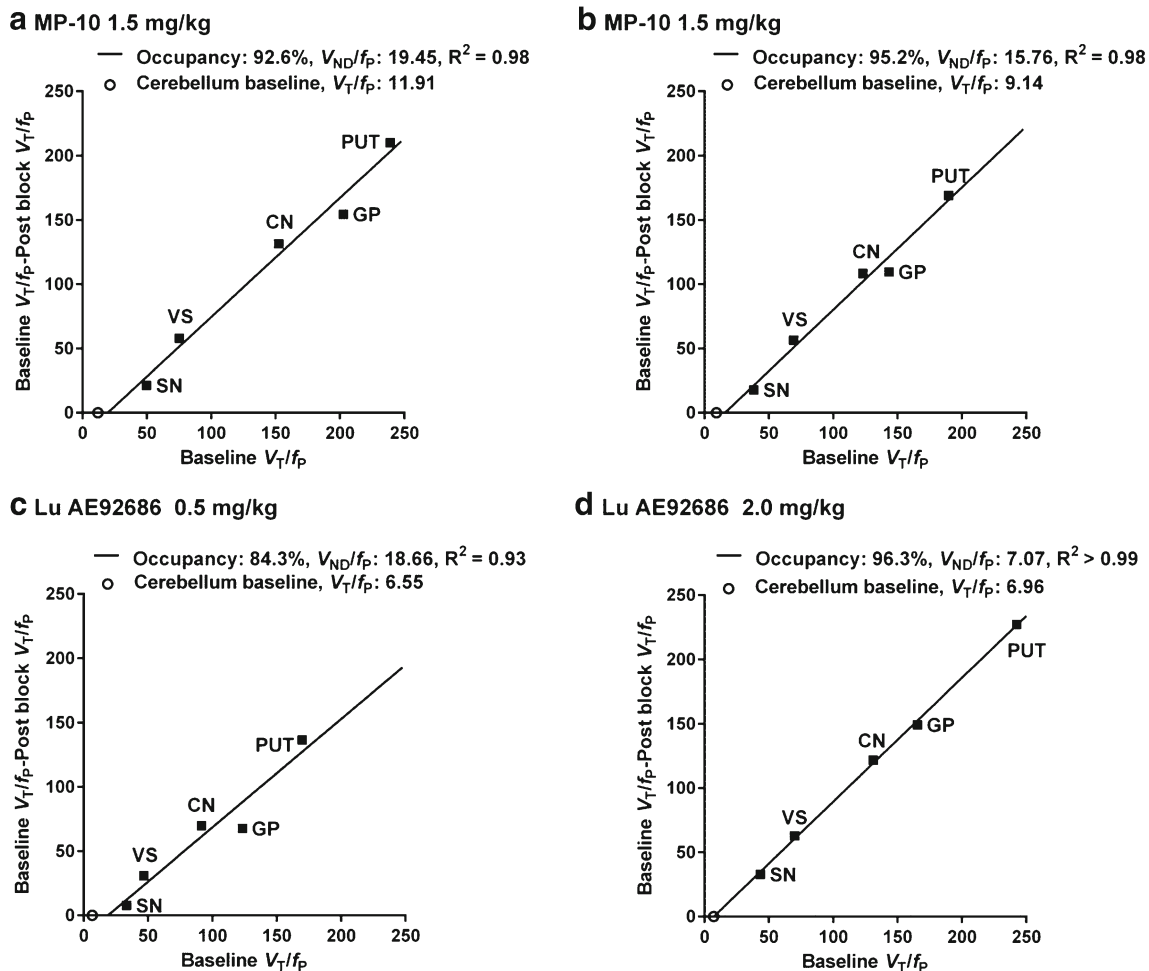
Fig. 7 Lassen plots using V_T/f_p values obtained during baseline conditions and after MP-10 or unlabeled Lu AE92686 pretreatment before injection of [^{11}C]Lu AE92686; the regression analysis included five target regions: putamen (PUT), caudate nucleus (CN), globus pallidum (GP), ventral striatum (VS) and substantia nigra (SN) while cerebellum (open circle) was not included in the regression model. (**a**) MP-10 1.5 mg/kg in NHP2 (**b**) MP-10 1.5 mg/kg in NHP1 (**c**) Lu AE92686 0.5 mg/kg (**d**) Lu AE92686 2.0 mg/kg

Table 3 V_T values for all baseline experiments ($n = 7$) by Logan plot analysis and comparisons to baseline BP_{ND} values estimated by different reference tissue models

| | V_T | %COV | BP_{ND} | | | % COV |
	Logan plots	Logan plots	Logan plots	SRTM	Loganref	SRTM
PUT	12.3 ± 4.5	3.8 ± 2.2	24.3 ± 6.7	15.0 ± 2.1	15.0 ± 2.3	2.2 ± 0.3
CN	7.2 ± 2.5	3.3 ± 2.6	13.8 ± 3.1	10.4 ± 1.3	10.0 ± 1.2	2.1 ± 0.4
GP	8.8 ± 2.5	7.9 ± 1.4	17.2 ± 3.4	11.2 ± 1.4	11.1 ± 1.4	3.6 ± 1.1
VS	3.6 ± 1.2	3.8 ± 2.6	6.5 ± 1.7	6.1 ± 1.1	5.7 ± 1.1	4.3 ± 1.2
SN	2.3 ± 0.5	7.7 ± 2.6	3.8 ± 0.8	3.7 ± 0.4	3.4 ± 0.5	8.9 ± 2.0
CB	0.5 ± 0.1	8.8 ± 1.0	NA	NA	NA	NA

Data presented as mean ± SD

COV the coefficient of variation, *PUT* Putamen, *CN* Caudate nucleus, *GP* Globus pallidum, *VS* Ventral striatum, *SN* Substantia nigra, *CB* Cerebellum, *SRTM* simplified reference tissue model, *Loganref* Logan reference tissue model, *NA* not applicable

discrepancies between estimated V_{ND}/f_p values and baseline cerebellum V_T/f_p values were possibly attributed to the noise in baseline V_T/f_p values. Such noise violates the assumption of noiseless data in the x-axis of the standard linear regression model in the Lassen plots used for calculation of occupancy [37]. Overall, these results support the use of cerebellum as a reference region in the quantification of [¹¹C]Lu AE92686 binding.

The TACs of the cerebellum were better described by the 2TCM than the 1TCM, similarly as has been described for several other PDE10A radioligands [10, 11, 14, 16, 18]. Possible explanations for this include a small fraction of specific binding, a kinetically distinguishable nondisplaceable compartment, tissue heterogeneity (gray and white matter), or a contamination from BBB-penetrating radiometabolites [38, 39]. A presence of BBB-penetrating radiometabolites was supported by the continuous increase in cerebellar V_T values with increasing PET measurement duration [40]. In contrast, V_T values in target regions remained stable with increasing PET measurement duration from 63 to 123 min.

Fig. 8 Representative results of simplified reference tissue model (SRTM) and Logan reference tissue model (Loganref) for 63 min data of [¹¹C]Lu AE92686 in one NHP (reference region: cerebellum). (**a**) SRTM fits in caudate nucleus (CN) and substantia nigra (SN) for baseline and Lu AE92686 2.0 mg/kg pretreatment condition (**b**) Loganref fits in CN and SN for baseline and Lu AE92686 2.0 mg/kg pretreatment condition (**c**) Bland-Altman plot; Difference of BP_{ND} (%) = [(SRTM - Logan plot analysis) / Logan plot analysis] × 100 (**d**) Linear regression analysis; dotted lines represent the line of identity
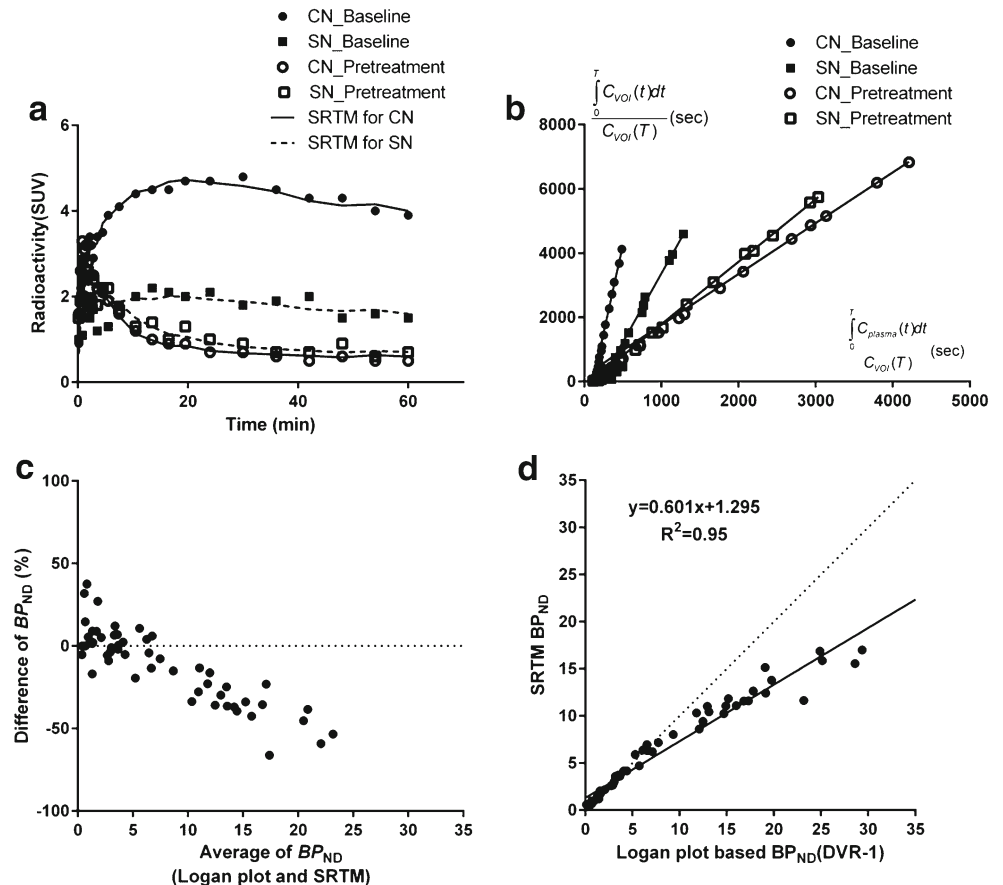
Table 4 Summary of PDE10A PET radioligands evaluated in primates[a]

Radioligand	Species	PreTx	Duration effect[c]	Reference region	PUT	SN	TRT (%)	Ref
[11C]Lu AE92686	Human (n = 6)	NA	NA	CB	7.5[d]	NA	6	9
	Cynomolgus (n = 2)	A[b]	NA	CB	6.5[d]	NA	NA	9
	Cynomolgus (n = 5)	A	A[b]	CB	15.0	3.7	NA	*
[11C]MP-10	Baboon (n = 4)	A	NA	CB	1.6	NA	NA	10
	Rhesus (n = 4)	A	NA	NA	NA	NA	NA	11
[11C]IMA107	Baboon (n = 2)	A	NA	CB	4.3	0.5[e]	NA	08/12
[11C]AMG 7980	Baboon (n = 2)	A	NA	Thalamus	0.8	NA	NA	13
[11C]T-773	Rhesus (n = 2)	A	NA	CB	2.2	NA	NA	14
[11C]TZ1964B	Cynomolgus (n = 2)	A[b]	NA	CB	4.6[d]	NA	NA	15
[18F]JNJ-42259152	Human (n = 12)	NA	A	Frontal ctx	3.5	0.4	5–12	16
[18F]MNI-659	Human (n = 5)	NA	A	CB	3.8	NA	5–8	18
[18F]AMG 580	Rhesus (n = 1)	NA	NA	Midbrain	2.9	NA	NA	19
	Baboon (n = 2)	NA	NA	Thalamus	NA	NA	NA	19

PreTx pretreatment experiment with PDE10A inhibitor or unlabelled radioligand, *NA* not applicable, *A* available, *CB* Cerebellum, *Frontal ctx* Frontal cortex, *PUT* BP_{ND} values in putamen, *SN* BP_{ND} values in substantia nigra, *TRT (%)* test-retest variability (%) for BP_{ND} values = $\left[\frac{|test-retest|}{\left(\frac{test+retest}{2}\right)}\right] \times 100$

[a] Based on the literature describing the quantification or characterization of the radioligands

[b] No arterial input function

[c] Effect of PET measurement duration on quantification

[d] BP_{ND} values in striatum

[e] Reported in a human study (n = 12, healthy subjects)

*Current study

Therefore, the potential BBB-penetrating radiometabolites mainly influenced the quantification of radioactivity for the cerebellum.

To minimize the potential contribution from radiometabolites, it is preferred to apply the shortest PET measurement duration, which is sufficient for reliable estimation of V_T values by Logan plot analysis. Using 63 min PET data, reliable V_T values could be derived by Logan plot analysis both in target regions and cerebellum. PET measurement duration shorter than 63 min resulted in variable and poor identifiable V_T estimates in several regions. Furthermore, it should be considered that due to the rapid decay of [11C] (half-life = 20 min), a longer measurement duration might introduce more noise both in the image and blood data. Shortening of the PET measurement duration has also been proposed for the application of other PDE10A radioligand, e.g. [18F]JNJ-42259152 in rats, to overcome the confounding effects from BBB-penetrating radiometabolites [17]. Therefore, 63 min is suggested as the preferred PET measurement duration for [11C]Lu AE92686 binding in cynomolgus monkeys.

The metabolic rate of [11C]Lu AE92686 in monkeys is similar to rats, but more rapid than previously reported in humans [9]. It is worth noting that we compared the fraction of unchanged [11C]Lu AE92686 to the total amount of radioactivity in plasma across species. This relative fraction of unchanged [11C]Lu AE92686 in plasma is dependent on the clearance rate of the radiometabolites in plasma, a rate which also may differ across species. However, in general, the potential difference in metabolic rate across species is consistent with less extensive metabolism in higher species, an observation previously reported for other radioligands [10, 11, 16, 17, 41].

The radiometabolites observed early in monkey plasma were more hydrophilic than [11C]Lu AE92686, similar as in rat and human [9]. These observations are consistent with the results of a metabolic soft-spot mass spectrometry analysis of Lu AE92686. After incubation in rat and human liver microsomes, only hydroxy and di-hydroxy metabolites were suggested, and all metabolites were more hydrophilic than the parent compound (unpublished data, data on file at Lundbeck). It has been reported that at 40 min post-injection, the amount of radiometabolites in rat brain is small (<15 %) [9]. It may thus be anticipated that the majority of radioactivity in the NHP brain at 60 min post-injection would be [11C]Lu AE92686. Ideally, the structure of the metabolites would be identified and, if possible, the metabolites radiolabeled to examine their passage across the BBB. Further studies are warranted to characterize these radiometabolites and to further confirm their influence on the quantification of [11C]Lu AE92686 in the NHP brain.

A large number of PET radioligands have been developed for the PDE10A enzyme [8–19]. Table 4 summarizes the characteristics of PDE10A radioligands that have been applied in primates. After adjustment for the differences in target VOI (putamen vs. striatum) and PET measurement duration (63 min vs. 90 min), the striatal BP_{ND} values (12.0 ± 1.6) in the current study were 85 % higher than previously reported values with [^{11}C]Lu AE92686 in cynomolgus monkeys [9]. This difference may be caused by an enhanced striatum signal in the current study due to the resolution of the PET systems (1.6 mm vs. 3.5 mm) and to the use of a head fixation device, limiting head motion in the current study. Similar differences between PET systems have been reported in imaging studies of dopamine or serotonin transporters, with an increase in BP_{ND} values of up to 92 % when using the HRRT [42, 43]. It is noted that the majority of the studies of PDE10A radioligands did not in detail evaluate the influence of radiometabolites on quantification. For example, only studies using [^{18}F]JNJ-42259152 [16] or [^{18}F]MNI-659 [18] have examined the effect of PET measurement duration on the quantification, and for both radioligands an increase in V_T value was obtained with increasing PET measurement duration.

[^{11}C]Lu AE92686 binding in SN could be quantified with favorable signal to noise ratio. The BP_{ND} for SN was 3–5, which is higher than ~0.5 as reported in studies using other PDE10A radioligands and lower resolution PET systems [8, 16] (Table 4). A head-to-head comparison on the HRRT is required to allow for a direct comparison of SN binding by different PDE10A radioligands. In general, considering the relative small size of SN (56 ± 14 mm^3 in the current study), BP_{ND} values higher than 0.5 have been suggested to be required for reliable quantification [20]. The pretreatment studies in the current study confirm that the nondisplaceable binding in the SN is similar to that in the striatum. In conclusion, [^{11}C]Lu AE92686 may allow for the unique potential to quantify PDE10A binding in the SN. Such studies in nonhuman primates and humans may lead to a better understanding of the role of PDE10A in the pathophysiology and treatment of neuropsychiatric diseases.

A limitation of the current study is the use of anesthesia during PET measurements. The induction by ketamine and maintenance by sevoflurane is similar to the previously reported monkey study with [^{11}C]Lu AE92686 [9]. The influence of these anesthetics on the expression of PDE10A or cAMP concentration is to our knowledge not known. However, the striatal binding of [^{11}C]Lu AE92686 in awake humans and anaesthetized monkeys has been reported to be comparable in a previous study [9]. Therefore, the anesthesia effects on the binding of [^{11}C]Lu AE92686 are unlikely to be prominent.

In conclusion, our results suggest that [^{11}C]Lu AE92686 can be applied to examine PDE10A binding in striatum, GP and SN. A potential contribution from radiometabolites can be minimized by shortening the PET measurement duration to 63 min. Reliable BP_{ND} estimates could be derived by reference tissue models (SRTM and Loganref) and these models are the preferred methods in future pharmacological challenge studies in NHPs.

References

1. Wilson LS, Brandon NJ. Emerging biology of PDE10A. Curr Pharm Des. 2015;21(3):378–88.
2. Charych EI, Jiang L-X, Lo F, Sullivan K, Brandon NJ. Interplay of palmitoylation and phosphorylation in the trafficking and localization of phosphodiesterase 10A: implications for the treatment of schizophrenia. J Neurosci. 2010;30(27):9027–37.
3. Seeger TF, Bartlett B, Coskran TM, et al. Immunohistochemical localization of PDE10A in the rat brain. Brain Res. 2003;985(2):113–26.
4. Coskran TM, Morton D, Menniti FS, et al. Immunohistochemical localization of phosphodiesterase 10A in multiple mammalian species. J Histochem Cytochem. 2006;54(11):1205–13.
5. Giorgi M, Melchiorri G, Nuccetelli V, et al. PDE10A and PDE10A-dependent cAMP catabolism are dysregulated oppositely in striatum and nucleus accumbens after lesion of midbrain dopamine neurons in rat: a key step in parkinsonism physiopathology. Neurobiol Dis. 2011;43(1):293–303.
6. Nishi A, Kuroiwa M, Shuto T. Mechanisms for the modulation of dopamine D1 receptor signaling in striatal neurons. Front Neuroanat. 2011;5:43.

7. Kehler J, Nielsen J. PDE10A inhibitors: novel therapeutic drugs for schizophrenia. Curr Pharm Des. 2011;17(2):137–50.

8. Niccolini F, Foltynie T, Marques TR, et al. Loss of phosphodiesterase 10A expression is associated with progression and severity in Parkinson's disease. Brain. 2015;138(10):3003–15.

9. Kehler J, Kilburn JP, Estrada S, et al. Discovery and development of 11C-Lu AE92686 as a radioligand for PET imaging of phosphodiesterase10A in the brain. J Nucl Med. 2014;55(9):1513–8.

10. Plisson C, Salinas C, Weinzimmer D, et al. Radiosynthesis and in vivo evaluation of [11 C] MP-10 as a positron emission tomography radioligand for phosphodiesterase 10A. Nucl Med Biol. 2011;38(6):875–84.

11. Lin SF, Labaree D, Chen MK, et al. Further evaluation of [11C] MP-10 as a radiotracer for phosphodiesterase 10A: PET imaging study in rhesus monkeys and brain tissue metabolite analysis. Synapse. 2015;69(2):86–95.

12. Plisson C, Weinzimmer D, Jakobsen S, et al. Phosphodiesterase 10A PET radioligand development program: from pig to human. J Nucl Med. 2014;55(4):595–601.

13. Hwang D-R, Hu E, Rumfelt S, et al. Initial characterization of a PDE10A selective positron emission tomography tracer [11 C] AMG 7980 in non-human primates. Nucl Med Biol. 2014;41(4):343–9.

14. Takano A, Stepanov V, Gulyás B, et al. Evaluation of a novel PDE10APET radioligand, [11C]T-773, in nonhuman primates: brain and whole body PET and brain autoradiography. Synapse. 2015;69(7):345–55.

15. Liu H, Jin H, Yue X, et al. Preclinical evaluation of a promising C-11 labeled PET tracer for imaging phosphodiesterase 10A in the brain of living subject. Neuroimage. 2015;121:253–62.

16. Van Laere K, Ahmad RU, Hudyana H, et al. Quantification of 18F-JNJ-42259152, a novel phosphodiesterase 10A PET tracer: kinetic modeling and test–retest study in human brain. J Nucl Med. 2013;54(8):1285–93.

17. Celen S, Koole M, Ooms M, et al. Preclinical evaluation of [18F]JNJ42259152 as a PET tracer for PDE10A. Neuroimage. 2013;82:13–22.

18. Barret O, Thomae D, Tavares A, et al. In vivo assessment and dosimetry of 2 novel PDE10A PET radiotracers in humans: 18F-MNI-659 and 18F-MNI-654. J Nucl Med. 2014;55(8):1297–304.

19. Hwang D-R, Hu E, Allen JR, et al. Radiosynthesis and initial characterization of a PDE10A specific PET tracer [18 F]AMG 580 in non-human primates. Nucl Med Biol. 2015;42(8):654–63.

20. Laruelle M, Slifstein M, Huang Y. Relationships between radiotracer properties and image quality in molecular imaging of the brain with positron emission tomography. Mol Imaging Biol. 2003;5(6):363–75.

21. Perez-Costas E, Melendez-Ferro M, Roberts RC. Basal ganglia pathology in schizophrenia: dopamine connections and anomalies. J Neurochem. 2010;113(2):287–302.

22. Council NR. Guide for the care and use of laboratory animals. 8th ed. Washington, DC: The National Academies Press; 2011.

23. Verhoest PR, Chapin DS, Corman M, et al. Discovery of a novel class of phosphodiesterase 10A inhibitors and identification of clinical candidate 2-[4-(1-methyl-4-pyridin-4-yl-1H-pyrazol-3-yl)-phenoxymethyl]-quinoline (PF-2545920) for the treatment of schizophrenia. J Med Chem. 2009;52(16):5188–96.

24. Finnema SJ, Stepanov V, Ettrup A, et al. Characterization of [11C]Cimbi-36 as an agonist PET radioligand for the 5-HT2A and 5-HT2C receptors in the nonhuman primate brain. Neuroimage. 2014;84:342–53.

25. Finnema SJ, Halldin C, Bang-Andersen B, Bundgaard C, Farde L. Serotonin transporter occupancy by escitalopram and citalopram in the non-human primate brain: a [(11)C]MADAM PET study. Psychopharmacology. 2015;232(21–22):4159–67.

26. Varrone A, Sjöholm N, Eriksson L, Gulyás B, Halldin C, Farde L. Advancement in PET quantification using 3D-OP-OSEM point spread function reconstruction with the HRRT. Eur J Nucl Med Mol Imaging. 2009;36(10):1639–50.

27. Logan J, Fowler JS, Volkow ND, et al. Graphical analysis of reversible radioligand binding from time-activity measurements applied to [N-11C-methyl]-(−)-cocaine PET studies in human subjects. J Cereb Blood Flow Metab. 1990;10(5):740–7.

28. Lammertsma AA, Hume SP. Simplified reference tissue model for PET receptor studies. Neuroimage. 1996;4(3):153–8.

29. Logan J, Fowler JS, Volkow ND, Wang G-J, Ding Y-S, Alexoff DL. Distribution volume ratios without blood sampling from graphical analysis of PET data. J Cereb Blood Flow Metab. 1996;16(5):834–40.

30. Akaike H. An information criterion (AIC). Math Sci. 1976;14(153):5–9.

31. Cunningham VJ, Rabiner EA, Slifstein M, Laruelle M, Gunn RN. Measuring drug occupancy in the absence of a reference region: the Lassen plot re-visited. J Cereb Blood Flow Metab. 2010;30(1):46–50.

32. Zanderigo F, Ogden RT, Parsey RV. Reference region approaches in PET: a comparative study on multiple radioligands. J Cereb Blood Flow Metab. 2013;33(6):888–97.

33. Parsey RV, Slifstein M, Hwang D-R, et al. Validation and reproducibility of measurement of 5-HT1A receptor parameters with [carbonyl-11C]WAY-100635 in humans: comparison of arterial and reference tissue input functions. J Cereb Blood Flow Metab. 2000;20(7):1111–33.

34. Gunn RN, Sargent PA, Bench CJ, et al. Tracer kinetic modeling of the 5-HT1AReceptor Ligand [carbonyl-11C]WAY-100635 for PET. Neuroimage. 1998;8(4):426–40.

35. Sandiego CM, Gallezot J-D, Lim K, et al. Reference region modeling approaches for amphetamine challenge studies with [11C]FLB 457 and PET. J Cereb Blood Flow Metab. 2015;35(4):623–9.

36. Finnema SJ, Scheinin M, Shahid M, et al. Application of cross-species PET imaging to assess neurotransmitter release in brain. Psychopharmacology. 2015;232(21):4129–57.

37. Guo Q, Owen DR, Rabiner EA, Turkheimer FE, Gunn RN. A graphical method to compare the in vivo binding potential of PET radioligands in the absence of a reference region: application to [11C]PBR28 and [18F]PBR111 for TSPO imaging. J Cereb Blood Flow Metab. 2014;34(7):1162–8.

38. Lammertsma AA, Bench CJ, Hume SP, et al. Comparison of methods for analysis of clinical [11C]Raclopride studies. J Cereb Blood Flow Metab. 1996;16(1):42–52.

39. Shrestha S, Hirvonen J, Hines CS, et al. Serotonin-1A receptors in major depression quantified using PET: controversies, confounds, and recommendations. Neuroimage. 2012;59(4):3243–51.

40. Zoghbi SS, Shetty HU, Ichise M, et al. PET imaging of the dopamine transporter with 18F-FECNT: a polar radiometabolite confounds brain radioligand measurements. J Nucl Med. 2006;47(3):520–7.

41. Pike VW. PET radiotracers: crossing the blood–brain barrier and surviving metabolism. Trends Pharmacol Sci. 2009;30(8):431–40.

42. Leroy C, Comtat C, Trebossen R, Syrota A, Martinot JL, Ribeiro MJ. Assessment of 11C-PE2I binding to the neuronal dopamine transporter in humans with the high-spatial-resolution PET scanner HRRT. J Nucl Med. 2007;48(4):538–46.

43. Schain M, Tóth M, Cselényi Z, et al. Improved mapping and quantification of serotonin transporter availability in the human brainstem with the HRRT. Eur J Nucl Med Mol Imaging. 2013;40(2):228–37.